




Soda-lime glass as biocompatible material to fabricate capillary-model devices by laser technologies

M. AYMERICH,¹ J. R. VÁZQUEZ DE ALDANA,² D. CANTELI,³ C. MOLPECERES,³ E. ALVAREZ,^{4,5} C. ALMENGLÓ,⁴ AND M. T. FLORES-ARIAS^{1,*} 

¹Photonics4Life Research Group, Departamento de Física Aplicada, Facultad de Físicas and Institute of Materials iMATUS, Universidade de Santiago de Compostela, 15782, Santiago de Compostela, Spain

²Aplicaciones del Láser y de la Fotónica Research Group, Departamento de Física Aplicada, Facultad de Ciencias, Universidad de Salamanca, 37008, Salamanca, Spain

³Centro Láser UPM, Universidad Politécnica de Madrid, Crta. de Valencia km 3.7, 28031, Madrid, Spain

⁴Instituto de Investigación Sanitaria de Santiago de Compostela (IDIS). Complejo Hospitalario Universitario de Santiago de Compostela (CHUS). SERGAS. Travesía da Choupana s/n, Santiago de Compostela, 15706 A Coruña, Spain

⁵Farmacología, Farmacia y Tecnología Farmacéutica Department. Universidade de Santiago de Compostela. 15782 Santiago de Compostela and CIBERCV, Spain

*maite.flores@usc.es

Abstract: Microfluidic devices have been widely developed in the last decades because of the huge number of fields where they can be applied. Among all the different fabrication techniques available, laser direct writing stands out since it is a fast, accurate, versatile and non-contact method. It is particularly well-suited when working with glass, a robust and cost-efficient material. These laser advantages allow the direct fabrication of not only high quality single microchannel devices but also complex and bifurcated structures. This work establishes a roadmap for manufacturing capillary-model devices with good biocompatibility in soda-lime glass substrates with pulsed lasers operating in the nanosecond, picosecond and femtosecond temporal range. We determine the optimal laser parameters required for fabricating channels with a diameter:depth rate of 2:1, keeping a semi-circular section. The presence of tin doping (~2%) in the soda-lime glass is shown to enable the fabrication with nanosecond pulses, and to improve the quality of the channels, reducing the cracking at the sides, when picosecond or femtosecond pulses were used. On the other hand, two regimes of surface roughness are found: a low roughness regime for channels fabricated with nanosecond lasers and a high roughness regime for those fabricated with pico and femtosecond lasers. Human umbilical vein endothelial cells (HUVEC) are employed for cell culturing for evaluating the biocompatibility of the channels. Structures manufactured with the nanosecond laser resulted more suitable in terms of cell adhesion than those fabricated with the picosecond and femtosecond lasers, due to the different surface roughness regimes obtained. In order to increase the biocompatibility of the channels fabricated with pico and femtosecond lasers and to improve the cell growth, a controlled post-thermal treatment is carried out for smoothing the surface.

© 2022 Optica Publishing Group under the terms of the [Optica Open Access Publishing Agreement](#)

1. Introduction

Organ-on-a-chip devices and 3D in-vitro microfluidic models aroused a huge interest in research in the last decades. These devices offer the opportunity of mimicking biological systems in laboratory conditions for performing biomedical assays, leading to a better understanding of different pathologies. The main characteristic of lab-on-a-chip devices, total analysis systems and other fluidic devices is the miniaturization of fluidic problems for performing assays in

controlled environments [1]. The development of these devices was a direct consequence of the expansion of the microfluidics field concerning applicability and fabrication terms, having significant interest in different fields such as Biology, Chemistry or Medicine.

In particular, organ-on-a-chip models are very promising since they allow the imitation of cellular environments in-vitro conditions. In literature, different models of organ-like structures can be found. For example, Jang and Suh [2] analysed renal cells behavior by using a multilayer microfluidic device, demonstrating its potential for drug screening and tissue engineering. Lee et al. [3] fabricated a fluidic chip for hepatocyte culture for drug toxicity studies and Kimura et al. [4] presented an in vitro microfluidic chip for the motorization of gut models. Fabrication of dynamic coronary bifurcation models for the study of the endothelium has already been reported [5] and organ-on-a-chip devices were employed for the study of fluid dynamics and the impact of vessel geometry in cell deposition [6].

Organ-on-a-chip devices are very useful in the research of different pathologies, from cardiovascular to tumour ones. Wang et al. [7] employed fluidic devices to analyse cell alignment and endothelium inflammatory response to the flow direction and its correlation with atherosclerotic plaque formation. Song et al. [8] studied tumor cell deposition by using fluidic devices, using microfluidic chips to mimic the vasculature and to study the interaction between the endothelium and metastatic breast cancer cells. Chung et al. [9] employed these devices for studying angiogenesis and cell to cell interactions for liver tissue engineering. Moreover, these chips have been employed for several years for the evaluation of drug distribution dynamics. One example can be found in [10] where Ghaemmaghami et al. reported different organ models for this purpose.

In particular, the imitation of capillary networks is specially interesting for the in vitro study of flow dynamics of microcirculation. Kim et al. [11] fabricated a three-dimensional matrix that mimics the human microvasculature for pharmaceutical screening. Fujiwara et al. [12] employed the model of a stenosed channel for the study of the motion of red cells. Also, Shevkopyas et al. proposed years ago a fabrication technique for a network that mimics mammalian circulation [13].

In this particular setting, one of the most important disadvantages of the mentioned models is the difficulty to obtain circular profiles instead of rectangular ones. Shiu et al. [14] presented a fast and efficient technique for channel fabrication but the resulting structures had a rectangular section that is not suitable for imitating a blood vessel. Another disadvantage of some techniques is the non-realistic surfaces obtained with perfectly smooth surfaces that cannot biologically imitate the intrinsic irregularities of blood vessels. Moreover, it is common to find the limitation of the structure to a single and straight microchannel and the complex vascular tree structure is not always replicated. For example, Osaki et al. [15] cultured endothelial cells over collagen channels for studying the cell migration, but the structure was limited to simple channels. Among others, the limitations previously mentioned mainly come from the fabrication process.

Originally, fluidic devices came from the micro-electro-mechanical systems (MEMS) field and applied the existing fabrication techniques to optical and fluidic problems. Nowadays, the manufacture procedures for obtaining these devices, as well as the materials employed, has broadly increased. Brambley et al. [16] used some well-known lithography technique, traditionally employed in MEMS, that presents high quality results but with the inconvenience of needing cleanroom facilities and numerous procedure steps. Other techniques, like hot embossing or injection molding are limited to the employment of only one kind of materials, resulting in being inefficient in comparison to others. For example, Hecke and Schomburg presented a topical review in this matter [17], but it was only limited to thermoplastic materials. Mali et al. [18] have reported the fabrication of structures by using electron beam lithography. They fabricated different microfluidic units in a fast way by using this technique. Nevertheless, electron beam lithography presents the inconvenience of expensive cost and long procedure time. Xia and

Whitesides described for the first time [19], a widespread technique for the fabrication of fluidic devices in soft-lithography, which is easy, quick and inexpensive. Fujii presented in [20] the use of this method with polydimethylsiloxane (PDMS) focused on biomedical applications. The PDMS is commonly employed as material to replicate structures from a master for microfluidic devices. McDonald et al. reported in [21] the suitability of PDMS for microfluidic device fabrication thanks to its biocompatibility and permeability. Nevertheless, Aymerich et al. analyzed in [22] that this material presented a significant drawback: when it was in contact with organic solvents it degraded, being non-optimal for applications that include chemistries. To avoid that problem, they employed sol-gel coating. Two-photon polymerization (TPP) has been also applied to the fabrication on functional three-dimensional micro-structures [23], in particular scaffolds for tissue engineering such as capillary models [24]. The impressive potential of this multiple-step technique for high-precision manufacturing is however limited in terms of the target materials that can be utilized for fabrication.

Laser direct ablation of substrates is presented as an advantageous technique for the manufacturing of these chips. Xu et al. fabricated microfluidic devices via direct laser ablation in the femtosecond regime, creating multifunctional units that can integrate in several configurations [25]. Ablation is a precise, accurate and fast method that has a non-contact nature. It is very versatile, allowing the fabrication of very different structures in a one step process, obtaining customizable devices with no need of expensive prototyping costs. Another advantage of laser ablation is that it can be performed in any material. Roberts et al. created microdiagnostic systems [26] by ultraviolet laser micromachining in polymers; Zhao and Shin fabricated microchannels in fused silica [27]; Sunderlal et al. studied the fabrication of channels in polycarbonate via laser direct writing [28] and Pan et al. manufactured these structures in glass [29]. Among all materials, glass substrates present numerous advantages that make them ideal for fabricating these kinds of fluidic devices. Glasses are hard, chemically stable and have good electrical and thermal properties. Carlen et al. [30] remarked that they have a low autofluorescence and they are transparent in the range of near-UV-visible-IR wavelengths, making this substrate ideal for lab-on-a-chip and organ-on-a-chip devices. Tanaka et al. reported in [31] that human endothelial cells can attach this material, which is a key factor for mimicking biological conditions.

In general, for the laser processing of glass targets two approaches can be followed depending on the main physical mechanisms which they rely on. The first approach is based on the linear absorption of the electromagnetic laser radiation, that leads to the heating of the target and the subsequent evaporation of the overheated material. A widely used laser family for glass processing under this approach is CO₂ laser, whose main emission wavelength is strongly absorbed by glass, and can operate in continuous wave or pulsed emission (Q-switched) [32]. The strongly thermal process easily produces cracking and affection of surrounding areas of the sample. Another family of lasers that can be used in this approach are solid state nanosecond lasers. However, typical central wavelength of nanosecond laser pulses is the range of ~1 μm (Nd-based lasers), lying in the transparency window of glasses and, therefore, the energy transfer to the target is negligible. The ablation is still possible, but it is linked to the presence of defects that may initiate the ablation process, and typically require very large fluences and leads to cracking and severe damage of the surroundings. To overcome this problem, one possibility consists of reducing the operation wavelength by non-linear frequency conversion in crystals down to the visible or ultraviolet spectral region, in such a way that linear absorption may induce the efficient energy deposition in the sample. As main drawbacks of this approach we should mention the modal quality degradation, the increase in the shot-to-shot instability, and the significant power reduction derived from the nonlinear processes. Other possibilities are based on indirect energy transfer approaches [33] and consist of locating a highly absorbing material near the surface of the glass sample that may transfer the absorbed energy to the glass. These techniques are, for instance, laser-induced backside wet/dry etching (LIBWE, LIBDE) [34] or laser-induced plasma-assisted

ablation (LIPAA) [35], but they require the sample preparation, the precise optimization of both targets and results are, in general, less controllable. However, high-quality direct ablation of glass targets with ns IR pulses is possible when the sample has a small amount of dopants [36,37] that may initiate the energy deposition process: in such case, the energy transfer becomes efficient and high-quality processing of arbitrary-shape channel structures can be produced with good control on the geometry.

The second general approach is based on the non-linear absorption of the laser radiation due to strong-field ionization processes (multiphoton or tunnel ionization) [38], and it is named ultrafast ablation. To initiate such non-linear processes, high peak intensities are required and, therefore, the use of ultrashort laser pulses in the picosecond or femtosecond regime are needed. The main advantage of this technique is the minimum collateral damage of the sample due to the ultrashort temporal regime of the laser-matter interaction [39], that prevents the transfer of energy and heat diffusion, thus allowing high-precision structuring of almost any transparent target and, therefore, the fabrication of surface channels in a single step process. Moreover, the possibility to produce localized damage in the volume of glass has opened the door to the development of 3D embedded fluidic devices by using a chemical etching after irradiation [40].

In this work, we present for the first time, to our knowledge, a comparison among channels fabricated in the three pulse duration regimes, all of them performed in the surface of commercial soda-lime glass, provided by a local supplier, by direct laser ablation in the infrared spectral range. The aim of these structures is the imitation of capillary networks as in organ-on-a-chip devices that will allow the study of fluid dynamics inside the device, and for that reason it is crucial keeping a semi-circular section of the channels. The possibility to have a roadmap for laser fabrication of devices in glass with different laser systems will allow researchers to know the characteristics of the devices that can be obtained by laser ablation, regarding the pulse duration employed as well as to select the most suitable laser systems for one specific application. These devices have a semi-circular profile and laser technologies allow fabricating geometries much more complex than a single straight channel. The optimal irradiation parameters and the minimum number of laser scans are determined in order to obtain channels with an appropriate diameter:depth ratio for each pulse duration regime used. These structures are characterised and compared. The influence of tin impurities present in the commercial soda-lime glass is analysed in the quality of the final channel. Derived from the fabrication process, certain roughness is generated on the channel walls that helps to imitate a more realistic biological environment. Since these structures act as capillary models, walls are covered by endothelial cells in order to obtain an in-vitro cell model. The endothelial cells growth over soda-lime glass substrates with different roughness values is evaluated in order to determine the most optimal roughness for proper cell adhesion to the surface. The generated roughness can be modified in a controlled manner thanks to post thermal treatments, enhancing the attachment of the cells to the channel walls. Section 2 presents materials and methods. Main results and discussions are presented in Section 3, combining the fabrication procedure for the capillaries-like devices, the modification of their surface roughness and the study of cell response over different values of roughness, corresponding to the different setup presented. Section 4 is devoted to the conclusions of the work.

2. Experimental set-up and materials

For the capillary-like structures, microchannels were fabricated with three laser systems with different pulse durations. In the nanosecond (ns) regime, a Q-switched Rofin Nd:YVO₄ laser with 20 ns pulse duration and 1064 nm wavelength was used. The output beam was conducted and scanned via a galvanometer system. A flat field lens (100 mm focal length) with a working area of 80 × 80 mm² was used for focusing. Beam radius at focal length was around 9 μm. A Lumera Super Rapid-HE (Nd:YVO₄) picosecond laser with pulse duration of 12 ps and 1064 nm

wavelength was employed for micromachining in the picosecond temporal regime. In this case, the sample was moved over a motorized table and the beam remained still, with a beam radius of 16 μm . For the femtosecond (fs) regime, an amplified Ti:Sapphire laser (Spectra Physics, Spitfire) with pulse of 100 fs duration and central wavelength of 800 nm was employed. This system operated at 1 kHz repetition rate. The nearly Gaussian beam was focused by an achromatic lens with 200 mm focal length, obtaining a beam radius of 11 μm . The sample was also fixed over a computer-controlled 3-axes motorized stage.

Cheap, common soda-lime glass substrates provided by a local supplier were used to fabricate the microchannels. The transmission spectrum was analysed by using a PerkinElmer Lamb 25 spectrometer, showing an absorption edge around 300 nm and high transmittance around 70% in the 350-1100 nm range. Also, a scanning electron microscope (Zeiss FESEM-Ultra Plus) with an energy dispersive X-ray (EDX) module was employed for analysing the chemical composition (see Table 1) of the soda-lime glass surfaces.

Table 1. Chemical composition of both sides of the employed glass (%)

	Undoped surface	Doped surface
Oxygen	50.25	48.97
Silicon	33.8	32.34
Sodium	9.08	9.14
Calcium	4.87	4.91
Magnesium	2.19	2.24
Aluminium	0.54	0.49
Tin	0.0	1.90

The soda-lime glass spectrum shown in Fig. 1, reveals that this material is highly transparent for the infrared wavelengths where the three laser systems operate. Transmittance values of 69% at and 73% are found for wavelengths of 1064 nm and 800 nm, respectively. Table 1) shows that silicon dioxide (SiO_2) is the principal component in this glass also sodium oxide (Na_2O) and calcium oxide (CaO). The EDX analysis reveals that there is a significant difference between both sides of the material: in one side of the glass there is a presence of tin, whereas in the other one there is not. These impurities derive from the float glass fabrication process and appear in all the flat soda-lime glasses. They derive from the fabrication process of this floating glass. In the first steps of its fabrication, all the raw materials are mixed and melted into a furnace that reaches temperatures up to 1500 $^\circ\text{C}$. Then, the molten glass is floated over a film of molten tin in order to cool down, obtaining a plane sheet of glass with uniform thickness. Transference of tin to the side of the glass that is in contact with the metal occurs during this process and, as we will see later and has already been described by Nieto et al. [37], the presence of this dopant will play a key role in laser ablation of the material.

A static furnace Nannetti-Faenza was used for carrying out the thermal treatment of the microchannels. The characterization and measurement of the samples was made by optical (Nikon MM-400) and confocal microscopy (Sensofar S Neox and Leica DCM 3D), as well as by the SEM microscope Zeiss FESEM-Ultra Plus already mentioned.

Human umbilical vein endothelial cells (HUVEC) were employed for the cell culture. Cells were obtained from the umbilical cords voluntarily donated from the mothers after signing the informed consent approved, as well as the protocol, by the Galician Ethics Committee for Human Studies (Spain). Following the protocol described by Rodiño et al. [41] cells were isolated and cultured, employing an endothelial growth medium (EGM-2, Lonza, Basle, Switzerland) with gentamicin/amphotericin B. Cells were treated under standard conditions. HUVECs were stained with calcein AM (1 μM ; Invitrogen, Thermo Fischer Scientific, Waltham, MA, USA) for 15 min

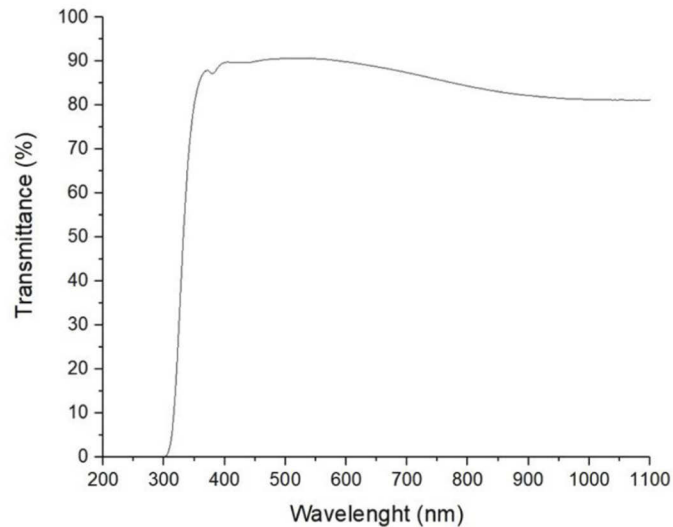


Fig. 1. Transmission spectrum of commercial soda-lime glass, ranging from 190 to 1100 nm wavelength.

in the dark at 37 °C. Calcein AM is a cell-permanent dye that acts as a viability indicator. For sterilization purposes, soda-lime glass samples were treated with an autoclave for 30 minutes at 120 °C and received a pre-treatment of gelatine 0.2% for 30 minutes prior to the cell seeding.

3. Results and discussion

In this section, the fabrication of microchannels in the near-infrared spectral range using different temporal regimes is presented. The characteristics of fabricated channels were analysed and compared. A post-thermal treatment was applied to modify the morphology of the channel and to decrease its roughness value, produced by the ablation process itself. Finally, HUVECs were cultured in the soda-lime microchannels in order to analyse cell behaviour regarding the surface roughness obtained with the different pulse regime lasers.

3.1. Laser microstructuring by direct writing

For the fabrication of the microchannels with different pulse durations, the setups shown in Fig. 2 were employed.

As it was shown in Table 1, the chemical composition of the surfaces of soda-lime glass was different. In one of the sides there was a presence of tin impurities derived from the fabrication process of glass (float glass). These dopants were a key in the microstructuring of the material with laser. For determining the better side to fabricate the channels, a comparison of the results when working with the doped and undoped surfaces, was made (see Fig. 3).

In Fig. 3(a) it can be seen that in the nanosecond regime impurities were essential for performing ablation. For short pulses, heat is a key factor for the final ablation; the material is first melted and then, it is vaporized. While working with the tin-doped surface, a high-quality microchannel was obtained and when irradiating the undoped surface with the same parameters, no material was removed. Tin dopants were critical to initiate the ionization of the material. If there was no presence of them, ablation did not occur. Previous works [42] demonstrated that if we work with a nanosecond laser the threshold energy for the undoped side of commercial glass is more than eight times higher than for the doped side. Working at the energy level required to microstructure

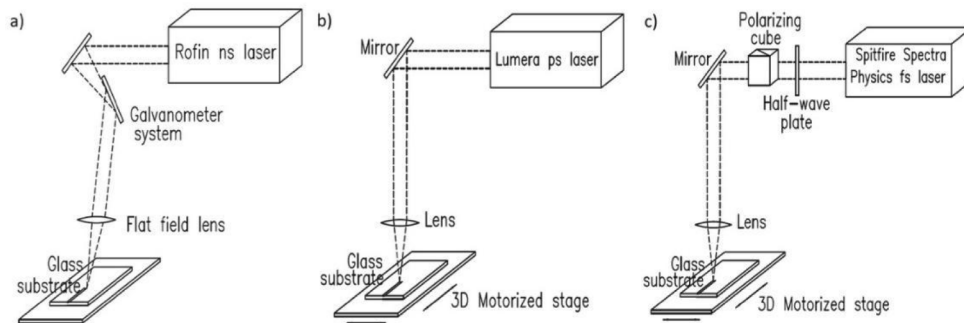


Fig. 2. Schemes of the setups employed for the fabrication of the channels by laser. a) Nanosecond, b) picosecond and c) femtosecond systems.

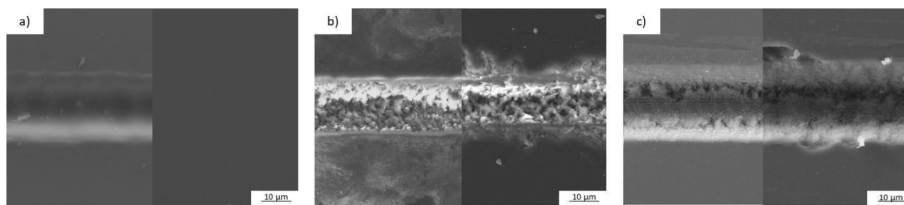


Fig. 3. Scanning electron microscopy images of the channels fabricated in both surfaces of the soda-lime glass sample when irradiating with the a) nanosecond, b) picosecond and c) femtosecond lasers. In each subpicture, left-side images correspond to the doped surface and right-side to the undoped surface.

the surface without tin would lead to the presence of cracks in the borders of the channel, which are typical when the laser fluence is high.

In picosecond and femtosecond regimes, Figs. 3(b) and 3(c) respectively, ablation occurs on both sides of the glass due to the physical mechanisms of ablation in those temporal regimes. Nevertheless, there were important differences in the morphological quality of the generated structures. Whereas in the doped side of the glass the channel shows straight and sharp edges (left-side images in Fig. 3), in the undoped one the structure presents several cracks and edge chipping (right-side images in Fig. 3). The formation of such defects in the micromachining of glasses with ultrashort pulses appears frequently and it is related to the low thermal diffusivity of these materials. High temperature gradients are created when heat is deposited in the beam focal volume. When there is not enough time for heat diffusion, mechanical fractures and cracks are created. Then, tin impurities present in the glass probably help to increase heat diffusion and minimize the formation of cracks and edge chips.

The processing parameters (pulse energy, repetition rate, beam size and number of scans) can be then optimized in order to prevent such defects from appearing and trying to get direct comparison in the morphology of the channels produced with the three laser systems. As the objective of the work is to obtain a rapid processing for fabricating microchannels that can be used in OOC, we prioritize the minimum time needed for obtaining these channels with a good final quality, without cracks, although the energy used in the case of picosecond and femtosecond laser was higher than needed for obtaining these channels with more than one laser scan. This assumption provokes a roughness at the walls of the channel higher than the one obtained with several laser scans. However, as we will show later, a convenient decrease of this roughness can be carried out in a controlled way if needed. Therefore, results observed in the undoped side of the sample are not surprising. In order to explain the Sn role in the excellent quality of the

microchannels fabricated on the doped side of the sample, we measured the threshold fluence in the case of pico and femtosecond pulses and channel dimensions in both sides, obtaining experimental values in the range of those reported in the literature [42]. It means that the presence of dopants has significant effect neither in the generation of the free-electron plasma during the pulse irradiation, nor in the critical density for producing ultrafast ablation. Then, the role of the Sn dopant in the morphology of the channels is not related with the initialisation of the ablation but is closely linked to an increase in the thermal diffusion of the irradiated volume of the glass, thus reducing the high temperature gradients created during the irradiation, and consequently minimizing the mechanical stresses that lead to the formation of cracks and edge chipping.

For determining the optimal laser parameters (specially in the surface with tin impurities) that ensure the homogenous ablation of a microchannel in soda-lime, a previous study of the processing setting was carried out with each laser system. Thresholds mean fluences were experimentally measured in the three scanning cases, considering them as the minimum fluence value that ablates in the material when pulses are not overlapped. This threshold value was 138 J/cm^2 , 49 J/cm^2 and 5 J/cm^2 for the nano, pico and femtosecond lasers, respectively. Notice in the case of the nanosecond laser, this value refers to the threshold corresponding to the doped face of the glass. Energy per pulse to ablate the microchannel was chosen in all cases as the double of the threshold energy. This decision was taken to ensure a homogenous ablation process along the channels and to manufacture the structures with the least possible scans, optimizing the process for mass production. As we previously said, it is important to notice that short and ultrashort pulse processing of transparent dielectrics depends on different physical phenomena: while linear or defect-induced absorption dominates in the short pulse case, nonlinear effects are huge in the ultrashort one. So, due to the different physical processes involved in laser machining with long and short pulses [43], the fluence needed for material removal decreases as the pulse duration becomes shorter. Optimal laser parameters for micromachining soda-lime glass in order to get a channel with the same aspect ratio with the lower number of laser scans were found as follows: for the ns laser $700 \mu\text{J}$ pulse energy, 10 kHz repetition rate and 50 mm/s scan speed, with a pulse overlapping of 73%; for the ps regime, parameters were $80 \mu\text{J}$ pulse energy, 10 kHz repetition rate and 20 mm/s scan speed, with a pulse overlapping of 96%; for the fs regime, $40 \mu\text{J}$ pulse energy, 1 kHz repetition rate and 0.6 mm/s scan speed were employed, with pulse overlapping of 97%.

The evolution of the channel dimensions with the number of laser scans was studied as it is shown in the graphics of Fig. 4. As expected, dimensions of the structures increase with the laser scans. Measurements were taken with a Sensofar S Neox confocal microscope and with a Nikon MM-400 measuring microscope when the depth of the channel was too large for the confocal inspections. Note that graphs a_1 , b_1 and c_1 in Fig. 4 have different axis limits.

As it is presented in the graphics of Fig. 4, the evolution of the depth and diameter of the channels was different depending on the temporal regime employed. In the case of nanosecond pulse duration (Figs. 4(a)), with the first laser scan, produced channels had a depth of around $1.5 \mu\text{m}$, and a plateau of around $8.8 \mu\text{m}$ was reached at the sixth laser scan. Between the fifth and sixth scans there was a jump in the amount of removed material. However, this jump could be explained due to a change in the mechanisms of ablation involved in the process, since the quantity of tin is expected to decrease as the deep of the channel increases although it remains present up to tens of microns [44]. The plateau obtained in the last scans may be due to the thermal nature of ablation in nanoseconds, where the material solidifies before final vaporization from the structure as it has already a significant depth and material cannot be ejected. The diameter of the microchannel increased with the scans from 19 to $28 \mu\text{m}$, from one to ten laser scans, respectively. For channels obtained with picosecond pulse duration (Figs. 4(b)), the depth achieved with one laser scan was around $8 \mu\text{m}$ and increased gradually with each laser scan until $60 \mu\text{m}$ in the tenth scan. In this case, no plateau was achieved. The diameter of the microchannel started with a value around $20 \mu\text{m}$ until a plateau of $24 \mu\text{m}$ in the sixth scan. Finally, in the

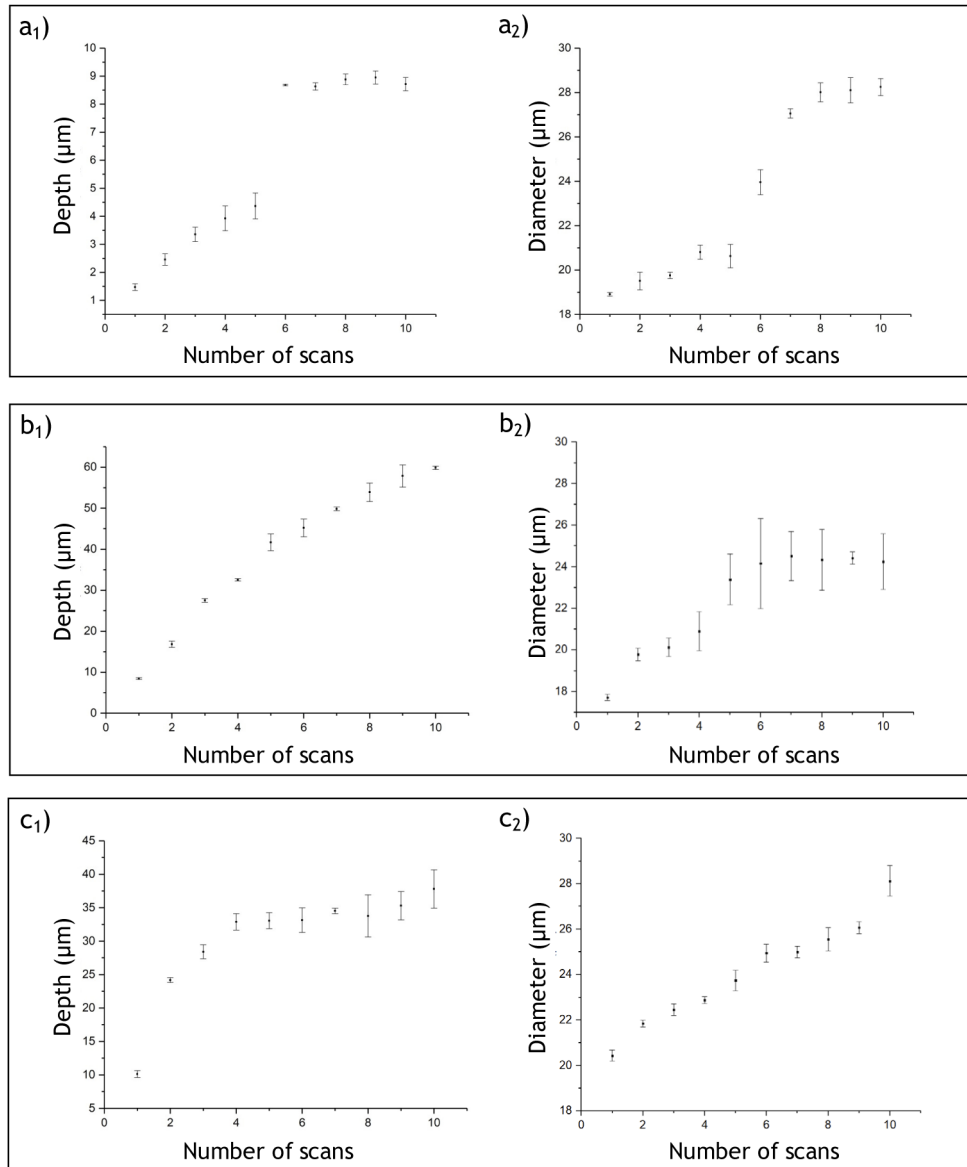


Fig. 4. Evolution of the depth (subscript 1) and diameter (subscript 2) of the channels when using a) the nanosecond b) the picosecond and c) the femtosecond temporal regimes.

femtosecond regime (Figs. 4(c)), with the first laser scan a channel with depth of 10 μm was obtained that increased up to 35 μm in the tenth laser scan. Diameters increased from 21 μm to 27 μm accordingly.

For comparison, we selected the best fabrication parameters in order to get microchannels with the same semi-circular aspect ratio for the three laser systems. Since the objective of the work is to optimize the manufacturing of channels for capillary microfluidic devices, it is effective to obtain the necessary aspect ratio with the least number of scans possible. For that reason we decided to use a pulse energy twice the threshold energy.

In the case of the nanosecond regime, several laser scans were needed to obtain a channel with the aimed dimensions. These channels show a smooth morphology and edges. With the ps and fs lasers we could obtain the channel with the desired aspect ratio just with one scan. The edges of the channels were well defined, which is typical of ultra-short pulse ablation. In the temporal regimes of ultrashort laser pulses, ablation could be achieved with less than twice the threshold energy, although the depth of the channels would be less. Working with these high energies led to a high roughness at the bottom of the channel. In the case of nanosecond pulsed laser, from Fig. 4, we see that six laser scans are the optimal number for obtaining a channel of $8.7 \pm 0.1 \mu\text{m}$ depth and $23.9 \pm 0.6 \mu\text{m}$ diameter. For the picosecond pulse duration laser, only one laser scan was needed obtaining a depth of $8.4 \pm 0.2 \mu\text{m}$ and $17.8 \pm 0.2 \mu\text{m}$ of diameter, as well as in the femtosecond regime, where a channel with $10.1 \pm 0.6 \mu\text{m}$ depth and $20.7 \pm 1.4 \mu\text{m}$ diameter was manufactured. In each case, three channels were manufactured and characterised in order to calculate the measurement errors (standard deviation).

Figure 5 includes SEM and three-dimensional confocal images of the structures. It can be appreciated that the microchannels fabricated with these different laser systems have similar dimensions and aspect ratio. Surface roughness of the structures was very different, as expected, due to the nature of the ablation process in the three temporal regimes. Surface arithmetical mean roughness (S_a) was calculated according to ISO 25178. S_a values were $178.7 \pm 15.6 \text{ nm}$, $1028.3 \pm 198.4 \text{ nm}$ and $1016.3 \pm 123.8 \text{ nm}$ for the nano, pico and femtosecond laser. In the nanosecond regime, the seed electrons present in the material gain energy from the laser and collide with the lattice or with bound electrons, promoting the generation of more released electrons. This process is known as avalanche ionization and results into the material breakdown and, subsequently, to its ablation. For shorter pulses (picosecond and femtosecond), seed electrons are not needed as they are produced by strong-field ionization processes (multiphoton or tunnel ionization) that may also be enhanced by collisional processes and avalanche ionization [43].

In the ultra-short range, removal results from a direct vaporization of the material with minimal heat affection and melting. Since we worked with a high energy value that ensures the channel fabrication in one scan, the process is then more disruptive and leads to a structure with a high roughness value but with sharp and well-defined borders, in contrast with the structures fabricated via nanosecond lasers. Picosecond laser ablation combines both effects, so part of the ablated material is vaporized and also heat is transferred to the lattice, resulting into a melting process. S_a of microchannels fabricated with pico and femtosecond lasers is higher due to the explosive nature of the process described above.

3.2. Thermal treatment

Once microchannels were fabricated with the three laser systems and characterised, thermal treatments were applied in order to modify their topography and to reduce in a controlled way their roughness. Thermal treatments have already been demonstrated to be useful for modifying the channel profile when manufacturing them with nanosecond laser direct writing [45]. In that work, the authors focused only on the fabrication of microstructures by nanosecond machining, while here, the procedure is adapted to the different laser temporal regimes. In this work thermal treatments were applied by using a Nannetti static furnace working at five different temperatures. Taking into account that the transition temperature for soda-lime glass is $570 \text{ }^\circ\text{C}$, the range of applied temperatures was from $590 \text{ }^\circ\text{C}$ to $630 \text{ }^\circ\text{C}$. Each sample was heated for two hours. As temperature rises, material melts and redistributes into the channel. Figure 7 plots the modification of the channel profile with the thermal treatments in each situation. Different microchannels were fabricated and subjected to thermal treatments at different temperatures. Table 2 records the roughness value variation of the microchannels with the temperature of the thermal treatment.

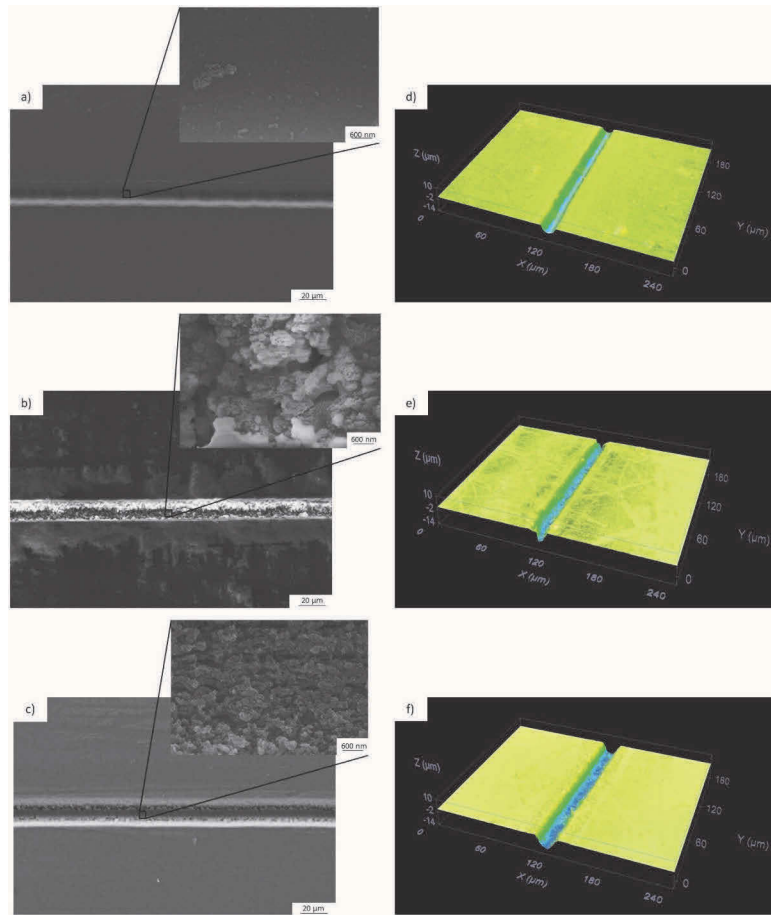


Fig. 5. Scanning electron microscopy and 3D confocal pictures of the manufactured structures with a) and d) nanosecond, b) and e) picosecond and c) and f) femtosecond lasers. Enlarged views of the bottom surface of each channel are shown at the top of the first column. All glass surfaces correspond to the side with tin impurities.

Table 2. Variation of S_a (following ISO 25178 regulation) for the microchannels after thermal

Roughness (nm)	Nanosecond	Picosecond	Femtosecond
No treatment	178.7 ± 15.6	1028.3 ± 198.4	1016.3 ± 123.8
590°C	136.1 ± 5.9	349.4 ± 35.1	184.1 ± 29.7
600°C	148.9 ± 1.4	232.6 ± 13.8	143.2 ± 13.7
610°C	140.3 ± 1.4	217.2 ± 27.4	102.4 ± 24.2
620°C	94.2 ± 24.2	117.9 ± 4.5	56.7 ± 17.5
630°C	12.1 ± 1.7	43.2 ± 1.6	12.9 ± 8.1

As can be observed in Table 2, the roughness values are very different for the nanosecond fabricated channels from those fabricated with pico and femtosecond lasers. In the first case, roughness below 200 nm is achieved by direct laser writing, we will name it “low roughness regime”. On the contrary, the ps and fs regimes produce surfaces with roughness above 1000 nm:

we will name it “high roughness regime”. In order to decrease the S_a value of these structures, the post-thermal treatment described in this work is performed.

Figure 6 shows the changes in the microchannels profiles when temperature is above the transition one. As material melt, channels become a shallower structure with a lower roughness value. Moreover, they became wider as the temperature increases. When working at 590 °C, all the channels approximately maintain the same aspect ratio as the non-treated ones. Nevertheless, for this temperature the structures generated with the picosecond and femtosecond lasers experienced a significant reduction of the surface roughness. As it was expected, as temperature increased, the depth of the channels decreased and the aspect ratio was modified, reaching a complete loss of their initial shape (630 °C). In that case, roughness took a value similar to non-processed glass.

All the structures manufactured with the different lasers can be employed for the imitation of different capillaries networks. Thanks to the laser versatility, plenty of designs can be performed with soda-lime glass, obtaining the structures that will allow the analysis of fluid dynamics inside these small blood vessels. For obtaining a sealed and closed device, a good option is to seal the glass device to a PDMS cover by plasma oxygen technique [46]. In this way, a proper fluidic device is obtained and both advantages of glass and PDMS are combined. On the one hand, glass confers robustness to the channel structure while the PDMS cover allows gas exchange when required for cell culture. In Fig. 7, some examples of different networks manufactured by direct laser ablation are shown. Here the capability of the laser technology to perform different geometries, including bifurcations, is depicted.

3.3. Evaluation of cell adhesion to the different roughness values

Capillary-like models, as it was mentioned in the Introduction, can be employed for studying the fluid behaviour and its role in the development of different pathologies. These studies can be limited to fluid perfusion but can also include the culture of endothelial cells in the inner walls of the channel structures in order to have a more realistic model of a capillary vessel, and to analyse the impact of fluid dynamics in the endothelium response. In the fabrication processes described in this paper, we have presented the manufacturing procedure of microfluidic devices via laser direct writing with several laser systems, detailing the topographic characteristics of the obtained microchannels. It is known that cell adhesion to a particular material depends on the kind of cell and, also, on the properties of the substrate. Ross et al. [47] describe roughness, elasticity and topography as some aspects that have a direct impact in cell adhesion. In the case of applications that require a 3D culture model of blood vessels in the capillary network dimensions, the impact of surface roughness value in cell response must be analysed. Fully glass devices are not the most suitable environment for long term cell cultures since they are not permeable to gases. When the analysis of fluid dynamics in capillaries networks is performed with the presence of cultured endothelial cells on their walls, a final device with a PDMS cover will ensure the gas permeability that the culture requires [48]. In order to see the impact of surface roughness in cell adhesion, HUVECs were cultured over two soda lime glass surfaces with roughness values corresponding to the low and high roughness regime explained above. HUVECs were cultured at standard conditions over the samples at a density of 10^5 cells/ml for one day. They were stained with calcein AM that indicates if cells are alive by means of green fluorescence (see Fig. 8).

Figure 8 shows the behaviour of endothelial cells over the soda-lime surfaces with different roughness values. In both images, cells are alive after one-day culture since they emit green fluorescence derived from calcein AM. Therefore, the biocompatibility of the surfaces is verified. The number of cells in both situations is approximately the same, meaning that cell growth is similar, and they seem to reach confluence in both cases. However, significant differences appear in cell morphology. Over the high roughness surface (Fig. 8(a)), endothelial cells have a more constrained and rounded shape, corresponding to a more stressed cell situation (see Fig. 8(a₂) magnification). On the contrary, in the case of the low roughness surface (Fig. 8(b)),

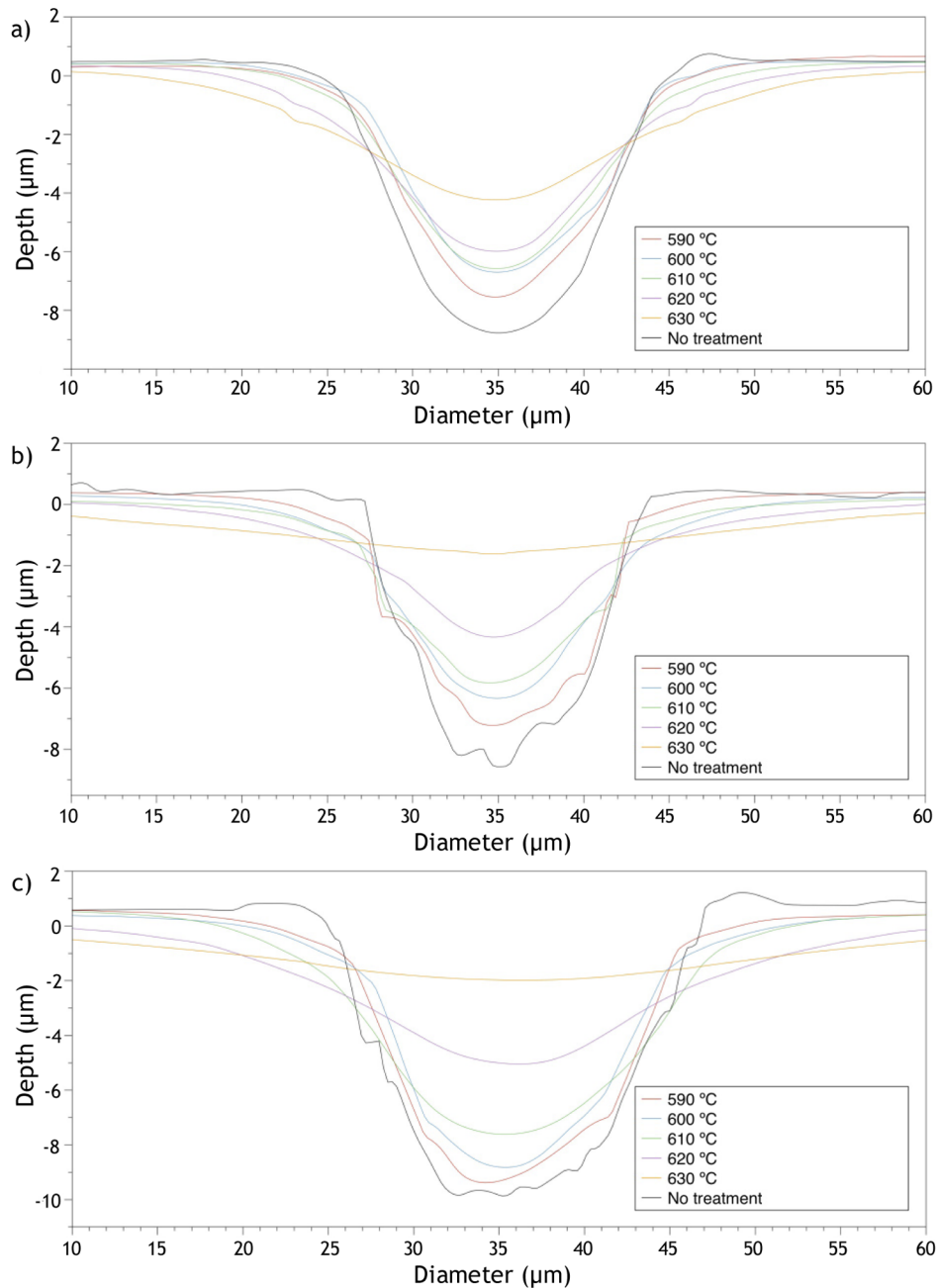


Fig. 6. Profile modification of the channels fabricated with the a) nanosecond b) picosecond and c) femtosecond laser systems with temperature.

HUVECs present a stretched morphology, showing individual cells covering more surface (see Fig. 8(b₂) magnification). Cell behaviour in this case is more physiological and endothelial cells reach a higher size than in the high roughness situation, where they are smaller and constrained. Endothelial cells under physiological conditions form a monolayer coating the internal part of the vasculature, where each cell expands to touch and interconnect with the membrane of its

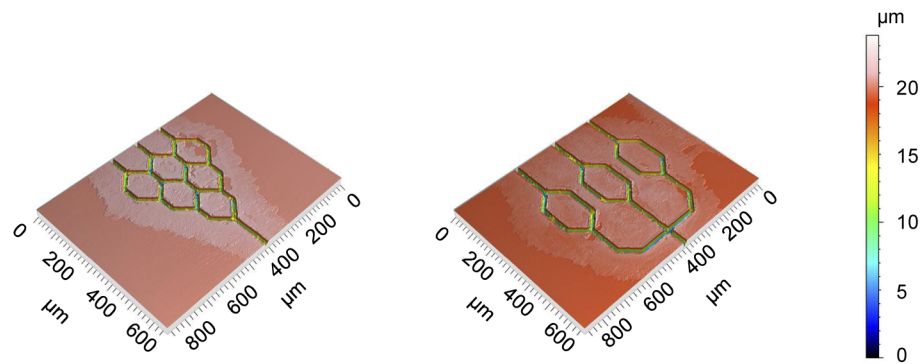


Fig. 7. Confocal 3D images of different capillaries-like devices manufactured with nanosecond pulse duration lasers on the tin doped surface of the glass.

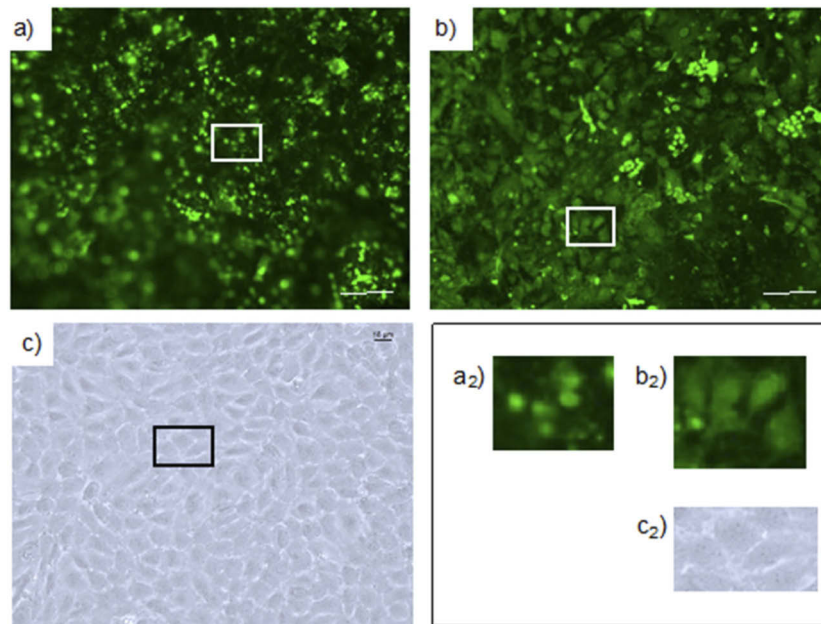


Fig. 8. Representative fluorescence microscopy images of HUVECs over soda-lime glass structures belonging to the a) high and b) low surface roughness regime; respectively. c) Representative phase-contrast image of HUVECs over conventional plastic surface for cell culture. a₂), b₂) and c₂) are magnifications of the respective squares marked on each original image. White scale-bar for a) and b) corresponds to 50 μm .

neighbour cells. When all the surface is covered by the monolayer the confluence state is reached and cells show the typical “cobblestone appearance” of endothelial cells (Fig. 8(c)). Therefore, we can say that low roughness laser-processed soda-lime glass surface leads to a better endothelial cells culture. This corresponds to the structures manufactured with the nanosecond laser system and to the microchannels that were subjected to different thermal treatments in order to reduce their roughness.

4. Conclusions

Fabrication of capillary like devices with soda-lime glass via direct writing laser has been presented. As the main element of these devices, microchannel structures have been fabricated with pulsed lasers operating in the near-infrared. In particular, lasers working in the three temporal regimes have been used: nanosecond, picosecond and femtosecond. The best laser parameters for each case were determined for obtaining the channels using the lower fabrication time, including the effect of the laser scans into the final dimensions of the structure. The result was a rounded profile channel that imitates the morphology of capillaries better than other fabrication processes that create rectangular profiles. It was found that impurities presented in the composition of glass are key factor not only in the case of using nanosecond laser as it is already known, but also when pico and femtosecond lasers were used since they avoided the crack formation. For the selected parameters, the surface roughness values were one order of magnitude higher for the channels fabricated with pico and femtosecond lasers than those fabricated with nanosecond lasers. Different thermal treatments were applied to the channels in order to modify in a controlled way the surface roughness of these structures. Since the final application of these chips is their employment as in-vitro models of capillary networks for the study of fluid dynamics, endothelial cells could be eventually cultured over their walls to have a more realistic environment. In this case, it was found that the channels with lower surface roughness values are more suitable for cell culture, in contrast with those with high roughness. In these smooth surfaces, endothelial cells presented a more physiological morphology and tempted to form a monolayer. Also, a low roughness surface is suitable for fluid dynamics assays since less optical scatter derives from the irregularities of the structure. So, considering the lower cost and robustness of commercial nanosecond equipment compared to ultrashort pulse systems, we can conclude that nanosecond lasers are enough for channel fabrication in tin-doped glass with direct use in biological applications. A similar behaviour is found for channels fabricated with pico and femtosecond lasers if a post-thermal treatment is applied, in order to decrease the surface roughness value.

Funding. Consejería de Educación, Junta de Castilla y León (SA136P20); Xunta de Galicia (IN607A2019-02); Consellería de Cultura, Educación e Ordenación Universitaria, Xunta de Galicia (ED431B 2020/29, ED431E 2018/08); Ministerio de Ciencia, Innovación y Universidades (EQC2018-004117-P, PID2020-119818); Agencia Estatal de Investigación (RTI2018-097063-B-100).

Acknowledgments. Authors gratefully thank contracts AEI RTI2018-097063-B-100, AEI/FEDER, UE; Ministerio de Economía y Competitividad, ED431B 2020/29 and ED431E 2018/08, Consellería de Educación Xunta de Galicia/FEDER, Consejería de Educación Junta de Castilla y León SA136P20, Xunta de Galicia, IN607A2019-02, Ministerio de Ciencia e Innovación PID2020-119818, Ministerio de Ciencia, Innovación y Universidades EQC2018-004117-P.

Disclosures. The authors declare no conflict of interest.

Data Availability. No data were generated in the presented research

References

1. Y. Temiz, R. D. Lovchik, G. V. Kaigala, and E. Delamarche, "Lab-on-a-chip devices: How to close and plug the lab?" *Microelectron. Eng.* **132**, 156–175 (2015).
2. K.J. Jang and K.Y. Suh, "A multi-layer microfluidic device for efficient culture and analysis of renal tubular cells," *Lab Chip* **10**(1), 36–42 (2010).
3. P.J. Lee, P. J. Hung, and L. P. Lee, "An artificial liver sinusoid with a microfluidic endothelial-like barrier for primary hepatocyte culture," *Biotechnol. Bioeng.* **97**(5), 1340–1346 (2007).
4. H. Kimura, T. Yamamoto, H. Sakai, Y. Sakai, and T. Fujii, "An integrated microfluidic system for long-term perfusion culture and on-line monitoring of intestinal tissue models," *Lab Chip* **8**(5), 741–746 (2008).
5. M. Aymerich, E. Álvarez, C. Bao-Varela, I. Moscoso, J.R. González-Juanatey, and M. T. Flores-Arias, "Laser technique for the fabrication of blood vessels-like models for preclinical studies of pathologies under flow conditions," *Biofabrication* **9**(2), 025033 (2017).
6. A. Otero-Cacho, M. Aymerich, M.T. Flores-Arias, M. Abal, E. Álvarez, V. Pérez-Muñuzuri, and A. P. Muñuzuri, "Determination of hemodynamic risk for vascular disease in planar artery bifurcations," *Sci. Rep.* **8**(1), 2795 (2018).
7. C. Wang, B.M. Baker, C.S. Chen, and M. A. Schwartz, "Endothelial cell sensing of flow direction," *Arterioscler., Thromb., Vasc. Biol.* **33**(9), 2130–2136 (2013).

8. J.W. Song, S. P. Caver, A. C. Walker, K. E. Luker, M. Gupya, Y. C. Tung, G. D. Luker, and S. Takayama, "Microfluidics endothelium for studying the intravascular adhesion of metastatic breast cancer cells," *PLoS One* **4**(4), e1–10 (2009).
9. S. Chung, R. Sudo, V. Vickerman, I. K. Zervantonakis, and R. D. Kamm, "Microfluidic platforms for studies of angiogenesis, cell migration, and cell-cell interactions," *Ann. Biomed. Eng.* **38**(3), 1164–1177 (2010).
10. M. Ghaemmaghami, M.J. Hancock, H. Harrington, H. Kaji, and A. and Khademhosseini, "Biomimetic tissues on a chip for drug discovery," *Drug Discov. Today* **17**(3-4), 173–181 (2012).
11. S. Kim, W. Kim, S. Lim, and J.S. Jeon, "Vasculature-on-a-chip for in vitro disease models," *Bioengineering* **4**(4), 8 (2017).
12. H. Fujiwara, T. Ishikawa, R. Lima, N. Matsuki, Y. Imai, H. Kaji, M. Nishizawa, and T. Yamaguchi, "Red blood cell motions in high-hematocrit blood flowing through a stenosed microchannel," *J. Biomech.* **42**(7), 838–843 (2009).
13. S.S. Shevkopyas, S. C. Gifford, T. Yoshida, and M.W. and Bitensky, "Prototype of an in vitro model of the microcirculation," *Microvasc. Res.* **65**(2), 132–136 (2003).
14. P. P. Shiu, G.K. Knopf, M. Ostojic, and S. Nikumb, "Rapid fabrication of tooling for microfluidic devices via laser micromachining and hot embossing," *J. Micromech. Microeng.* **18**(2), 025012 (2008).
15. T. Osaki, T. Kakegawa, T. Kageyama, J. Enomoto, T. Nittami, and J. and Fukuda, "Acceleration of vascular sprouting from fabricated perfusable vascular-like structures," *PLoS one* **10**, e0123735 (2015).
16. D. Brambley, B. Martin, and P.D. Prewett, "Microlithography: An overview," *Adv. Mater. Opt. Electron.* **4**(2), 55–74 (1994).
17. M. Hecke and W. K. Schomburg, "Review on micro molding of thermoplastic polymers," *J. Micromech. Microeng.* **14**(3), R1–R14 (2004).
18. P. Mali, A. Sarkar, and R. Lal, "Facile fabrication of microfluidic systems using electron beam lithography," *Lab Chip* **6**(2), 310 (2006).
19. Y. Xia and G.M. Whitesides, "Soft lithography," *Annu. Rev. Mater. Sci.* **28**(1), 153 (1998).
20. T. Fujii, "PDMS-based microfluidic devices for biomedical applications," *Microelectron. Eng.* **61-62**, 907–914 (2002).
21. J.C. McDonald, D. C. Duffy, J.R. Anderson, D.T. Chiu, H. Wu, O.J. Schueller, and G.M. Whitesides, "Fabrication of microfluidic systems in poly (dimethylsiloxane)," *Electrophoresis* **21**(1), 27–40 (2000).
22. M. Aymerich, A.I. Gómez-Varela, E. Álvarez, and M.T. Flores-Arias, "Study of different sol-gel coatings to enhance the lifetime of PDMS devices: evaluation of their biocompatibility," *Materials* **9**(9), 728 (2016).
23. C. Liao, A. Wuethrich, and M. Trau, "A material odyssey for 3D nano/microstructures: two photon polymerization based nanolithography in bioapplications," *Appl. Mater. Today* **19**, 100635 (2020).
24. A. Ovsianikov, S. Schlie, A. Ngezhayov, A. Haverich, and B.N. Chichkov, "Two-photon polymerization technique for microfabrication of CAD-designed 3D scaffolds from commercially available photosensitive materials," *J. Tissue Eng. Regener. Med.* **1**(6), 443–449 (2007).
25. B.B. Xu, Y.L. Zhang, H. Xia, W.F. Dong, H. Ding, and H.B. Sun, "Fabrication and multifunction integration of microfluidic chips by femtosecond laser direct writing," *Lab Chip* **13**(9), 1677–1690 (2013).
26. M.A. Roberts, J.S. Rossier, P. Bercier, and H. Girault, "UV laser machined polymer substrates for the development of microdiagnostic systems," *Anal. Chem.* **69**(11), 2035–2042 (1997).
27. X. Zhao and Y.C. Shin, "Femtosecond laser drilling of high-aspect ratio microchannels in glass," *Appl. Phys. A: Mater. Sci. Process.* **104**(2), 713–719 (2011).
28. S. Sunderlal, K. Sanasam, J. Alika, and N. Shrikrishna, "Fabrication of microchannel on polycarbonate below the laser ablation threshold by repeated scan via the second harmonic of Q-switched Nd:YAG laser," *J. Manufact. Processes* **55**, 359–372 (2020).
29. C. Pan, K. Chen, B. Liu, L. Ren, J. Wang, and Q. Hu, "Fabrication of micro-texture channel on glass by laser-induced plasma-assisted ablation and chemical corrosion for microfluidic devices," *J. Mater. Process. Technol.* **240**, 314–323 (2017).
30. E.T. Carlen, J.G. Bommer, J.W. Van Nieuwkasteele, and A. Van den Berg, "Silicon and Glass Micromachining," in *Lab-on-a-Chip Technology for Biomedical and Biological Applications*, K.E. Herold and A. Rasooly, eds., (Caister Academic, Norfolk: 2009), vol.1, pp. 83–114.
31. Y. Tanaka, Y. Kikukawa, K. Sato, Y. Sugii, and T. Kitamori, "Culture and leukocyte adhesion assay of human arterial endothelial cells in a glass microchip," *Anal. Sci.* **23**(3), 261–266 (2007).
32. C. Weingarten, Emrah Uluz, A. Schmickler, Karsten Braun, Edgar Willenborg, André Temmler, and Sebastian Heidrich, "Glass processing with pulsed CO₂ laser radiation," *Appl. Opt.* **56**(4), 777–783 (2017).
33. H. Liu, W. Lin, and M. Hong, "Hybrid laser precision engineering of transparent hard materials: challenges, solutions and applications," *Light: Sci. Appl.* **10**(1), 162 (2021).
34. J. Wang, H. Niino, and A. Yabe, "One-step microfabrication of fused silica by laser ablation of an organic solution," *Appl. Phys. A: Mater. Sci. Process.* **68**(1), 111–113 (1999).
35. T.U. Rahman, Z.U. Rehman, S. Ullah, H. Qayyum, B. Shafique, R. Ali, U. Liaqat, A.H. Dogar, and A. Qayyum, "Laser-induced plasma-assisted ablation (LIPAA) of glass: Effects of the laser fluence on plasma parameters and crater morphology," *Opt. Laser Technol.* **120**, 105768 (2019).
36. D. Nieto, M.T. Flores-Arias, G.M. O'Connor, and C. Gomez-Reino, "Laser direct-write technique for fabricating microlens arrays on soda-lime glass with a Nd: YVO₄ laser," *Appl. Opt.* **49**(26), 4979 (2010).

37. D. Nieto, J. Arines, and M.T. Flores-Arias, "Fluence ablation threshold dependence on tin impurities in commercial soda-lime glass," *Appl. Opt.* **53**(24), 5416–5420 (2014).
38. P. Balling and J. Schou, "Femtosecond-laser ablation dynamics of dielectrics: basics and applications for thin films," *Rep. Prog. Phys.* **76**(3), 036502 (2013).
39. B. C. Stuart, M. D. Feit, S. Herman, A. M. Rubenchik, B. W. Shore, and M. D. Perry, "Nanosecond-to-femtosecond laser-induced breakdown in dielectrics," *Phys. Rev. B* **53**(4), 1749–1761 (1996).
40. A. Marcinkevičius, S. Juodkakis, M. Watanabe, Miwa Ma., S. Matsuo, H. Misawa, and J. Nishii, "Femtosecond laser-assisted three-dimensional microfabrication in silica," *Opt. Lett.* **26**(5), 277–279 (2001).
41. B.K. Rodiño-Janeiro, M. González-Peteiro, R. Uceda-Somoza, J.R. González-Juanatey, and E. Álvarez, "Glycated albumin, a precursor of advanced glycation end-products, up-regulates NADPH oxidase and enhances oxidative stress in human endothelial cells: molecular correlate of diabetic vasculopathy," *Diabetes Metab. Res. Rev.* **26**(7), 550–558 (2010).
42. D. Nieto, J. Arines, G.M. O'Connor, and M.T. Flores-Arias, "Single-pulse laser ablation threshold of borosilicate, fused silica, sapphire, and soda-lime glass for pulse widths of 500fs, 10 ps, 20ns," *Appl. Opt.* **29**, 8596–8601 (2015).
43. X. Liu, D. Du, and G. Mourou, "Laser ablation and micromachining with ultrashort laser pulses," *IEEE J Quantum Electron.* **33**(10), 1706 (1997).
44. M.H. Krohn, J.R. Hellmann, C.G. Pantano, N.P. Lower, and R.K. Brow, "Effects of Tin on the Physical Properties and Crack Growth in Soda-Lime-Silica Float Glass," In: R.C. Bradt, D. Munz, M. Sakai, and K.W. White, eds., *Fracture Mechanics of Ceramics. Fracture Mechanics of Ceramics (Active Materials, Nanoscale Materials, Composites, Glass and Fundamentals)*, Springer, Boston, MA, vol 14. pp. 135–148 (2005).
45. D. Nieto, T. Delgado, and M.T. Flores-Arias, "Fabrication of microchannels on soda-lime glass substrates with a Nd:YVO4 laser," *Opt. Laser Eng.* **63**, 11–18 (2014).
46. S. Bhattacharya, A. Datta, J. M. Berg, and S. Gangopadhyay, "Studies on surface wettability of poly(dimethyl) siloxane (PDMS) and glass under oxygen-plasma treatment and correlation with bond strength," *J. Microelectromech. Syst.* **14**(3), 590–597 (2005).
47. A. M. Ross, Z. Jiang, M. Bastmeyer, and J. Lahann, "Physical aspects of cell culture substrates: Topography, roughness, and elasticity," *Small* **8**(3), 336–355 (2012).
48. K. Ziolkowska, E. Jedrych, R. Kwapiszewski, J. Lopacinska, M. Skolimowski, and M. Chudy, "PDMS/glass microfluidic cell culture system for cytotoxicity tests and cells passage," *Sens. Actuators, B* **145**(1), 533–542 (2010).